Charge and orbital order at head-to-head domain walls in $PbTiO_3$

K. Rahmanizadeh,* D. Wortmann, G. Bihlmayer, and S. Blügel

Peter Grünberg Institut (PGI-1) & Institute for Advanced Simulation (IAS-1), Forschungszentrum Jülich and JARA, D-52425 Jülich, Germany

(Received 19 May 2014; revised manuscript received 20 August 2014; published 2 September 2014)

At ferroelectric longitudinal domain walls there is an uncompensated charge, which could form a two-dimensional electron gas in the insulator. However, the uncompensated charges can be accommodated by, e.g., defects or localized states that split off from the conduction band. We carried out density functional theory calculations to study these scenarios in $PbTiO_3$ with and without consideration of strong correlation effects simulated via inclusion of a Hubbard parameter U. The optimized structure and electronic structure depend on the choice of this parameter: For vanishing U, a broad, conducting domain wall is obtained, while increasing U leads to localized Ti $3d$ states and an insulating, sharp domain wall. We also investigated the effects of varying the ferroelectric polarization on the electronic structure of these domain walls.

DOI: 10.1103/PhysRevB.90.115104 PACS number(s): 77.84.Cg, 77.22.Ej, 73.20.−r, 71.15.Mb

I. INTRODUCTION

Nowadays, investigations on perovskite oxide materials are an attractive challenge, due to the emerging novel electronic and magnetic properties at the surfaces or interfaces which do not exist in the corresponding parent bulk compounds. For example, a charge discontinuity at the interface of two simple band insulators $LaAlO_3$ and $SrTiO_3$ can induce conductivity at the interface [1], or a conductive domain wall forms in the insulating multiferroic $BiFeO_3$ [2]. These novel electronic and sometimes also the magnetic, properties are important for applications in nanoelectronics. Moreover, perovskite oxide materials are promising for energy applications: Thermoelectric or photocatalytic properties of these materials can be used for this purpose. For example, Nb or La-doped $SrTiO_3$ has a large thermoelectric power factor [3,4]. In addition, perovskite oxide materials have a good efficiency for photocatalytic water splitting. These compounds can be used for water splitting alone [5–7] or in combination with a good photolysis catalyst such as titania [8–10]. In all of these materials the electronic structure has a big impact on the energy efficiency.

In ferroelectrics, the electronic structure at surfaces, interfaces, or domain walls is different from the bulk. Electronic properties at the ferroelectric surfaces can be manipulated by switching the direction of the polarization perpendicular to the surface [11]. In ferroelectric thin films, the formation of a polarization perpendicular to the surface (out-of-plane polarization) is not stable without a further charge compensation mechanism. Out-of-plane polarizations induce charges at the surface that result in a depolarization field opposing the polarization, thereby suppressing ferroelectricity. To stabilize the ferroelectricity, the surface charges have to be screened or compensated, e.g., screening by two metallic electrodes in between which the ferroelectric material is placed stabilizes the polarization [12–14]. In a freestanding ferroelectric, the surface charge can be compensated by different surface charges (positive or negative) or by atomic and molecular adsorbates [15,16] controlled, for example, by different oxygen partial pressure [17]. In addition, polarization domains are formed with opposite orientations [18] for compensating the surface charges.

Similarly, 180° head-to-head domain walls (where the wall is perpendicular to the polar vector) are energetically costly due to electrostatic repulsion of dipoles. Although these longitudinal domain walls seem energetically not favorable, there is some experimental evidence about the existence of such domain walls [19,20]. Consequently, there are different ways to reduce the electrostatic energy at head-to-head domain walls. Possible mechanisms are the formation of a conducting layer, accumulation of defects, or changing the valency of the atoms at the domain wall. In a theoretical study, Wu and Vanderbilt stabilized a head-to-head 180° domain wall in $PbTiO_3$ by substituting certain layers of Ti atoms by acceptor or donor atoms like Sc or Nb [21].

In this paper, we study a head-to-head 180° domain wall in $PbTiO_3$ by means of density functional theory (DFT). The domain wall is modeled by a supercell and a thin-film setup. We investigate two methods for stabilizing a head-to-head domain wall: the formation of a conducting layer at the domain wall and, secondly, the localization of an electron on Ti by adding local correlation effects that are modeled by an on-site Coulomb repulsion parameter (Hubbard U). Finally, we present a thin-film model with varying defect concentrations at the thin-film surface, thereby modifying the polarization and the electronic structure in the head-to-head domain wall localized in the inner layers.

II. COMPUTATIONAL METHOD

The calculations have been performed using DFT in the generalized gradient approximation (GGA) [22] and, in some cases including the DFT+U model for the Ti d states. We employed the full-potential linearized augmented plane-wave (FLAPW) method as implemented in the FLEUR code [23].

The wave functions are expanded into augmented plane waves with a cutoff of $K_{\max} = 4.5\ (\text{a.u.})^{-1}$. For each structure, the muffin-tin radii (R_{MT}) were chosen as 2.10, 1.71, and 1.30 a.u. for Pb, Ti, and O, respectively. The Pb $5d$ states and Ti $3s$ and $3p$ states were treated as local orbitals. Self-consistency was considered to be achieved when the total energy variation from iteration to iteration did not exceed 10^{-6} htr and forces on the atoms were converged to 10^{-3} htr/a.u. The reciprocal space

*k.rahmanizadeh@fz-juelich.de

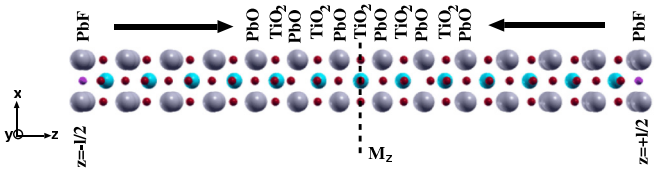

FIG. 1. (Color online) Relaxed structure of a longitudinal domain wall in $PbTiO_3$. Fluorine was used as an electron donor at the tail-to-tail domain wall. Large gray spheres represent Pb; the small (red) spheres are O atoms. The medium sized (blue) spheres represent Ti.

was sampled by a mesh containing 40 **k** points (corresponding to an $[8 \times 8 \times 8]$ Monkhorst-Pack mesh) in the irreducible Brillouin zone for the cubic (tetragonal) phases, and an equivalently dense **k**-point sampling for films.

The domain walls were calculated either in thin-film geometry or, for the p(1 × 1) in-plane unit cell in a supercell approach (see Fig. 1). In the thin-film calculations, the layers were embedded in semi-infinite vacuum. The advantage of this geometry over supercells is that the electrostatic boundary conditions can be easily changed and the out-of-plane degrees of freedom can be optimized without stress-tensor calculations. For the structural optimization, the in-plane lattice constant was then kept fixed to the theoretical optimized bulk value [24], while the remaining degrees of freedom were optimized. In the following section, we study domain walls with different charge and orbital order. This requires one to go beyond the structural model of a p(1 × 1) in-plane unit cell, e.g., to chose a c(2 × 2) cell if electrons are localized only on every second Ti atom at the interface or a p(2 × 2) unit cell if additionally orbital order effects are studied. Therefore, we group our results in subsections according to the chosen in-plane unit cells.

III. RESULTS

A. p(1×1) unit cells

The formation of a conducting layer at the head-to-head domain wall is one possibility to stabilize a longitudinal domain wall. The conduction layers screen the polarization charges at the domain wall, thereby stabilizing the ferroelectric domain. We simulated this mechanism by constructing a supercell with 13 formula units of $PbTiO_3$ and an in-plane p(1×1) unit cell. The purpose of this simulation is to investigate the electronic structure of the conducting layer.

We constructed the cell containing two domains with mirror symmetry at the domain walls (see Fig. 1). The mirror planes were placed at the head-to-head and the tail-to-tail domain walls at $z = 0$ and $z = \pm l/2$, respectively. The supercell contains two domains with six unit cells of bulk tetragonal $PbTiO_3$. The atomic positions in the supercell were initialized by relaxed positions of bulk tetragonal structure with polarization pointing in the $\pm z$ direction throughout the structure. The spontaneous polarization of $PbTiO_3$ is calculated by the Berry phase method as $87\mu C/cm^2$ [24]. This polarization P_s of the bulk structure induces a charge at the domain walls that amounts to $2aP_s$ (where a is the in-plane lattice constant) which is about 1.62 electron charges per in-plane unit cell. At the domain walls, the polarization can be screened by a

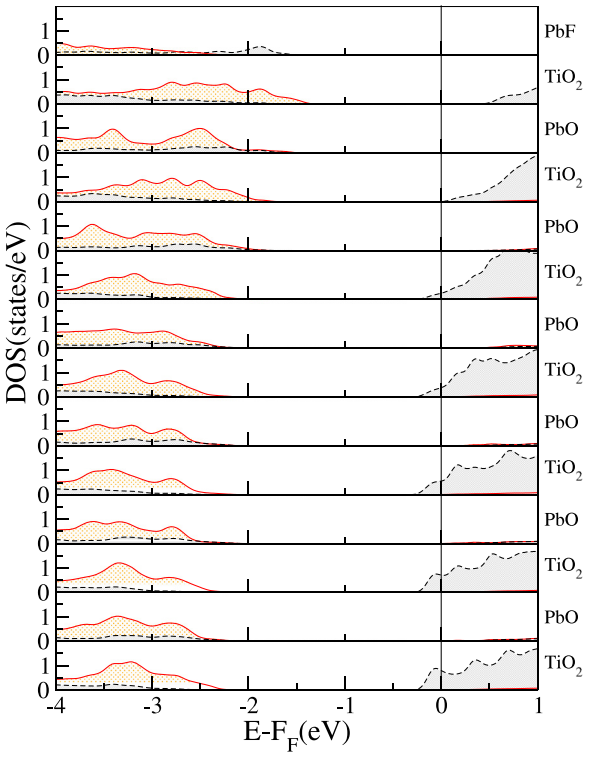

FIG. 2. (Color online) Layer-resolved density of states (LDOS) of a 5-nm domain with a longitudinal domain wall in $PbTiO_3$. The top and bottom panels show the DOS at the tail-to-tail and head-to-head domain walls, respectively. Full and dashed (red and black) lines represent DOS of the anions and cations in the layers, respectively. At the tail-to-tail wall a fluorine atom replacing the oxygen helps to stabilize the polarization in the domain.

conductive layer: at the head-to-head (HH) domain wall, the Fermi level (E_F) cuts the conduction band minimum, mainly formed by Ti d states. In the tail-to-tail (TT) wall, similarly holes are created when E_F reaches the valence band maximum, i.e., the oxygen p states. In this situation, the potential gradient between the HH and TT wall, that has to bridge the 3-eV bandgap, would lead to a depolarization field destroying the polarization. Therefore, at the TT wall we remove the holes by creating half an oxygen defect or replacing O by F, effectively introducing charge into the layer. Whether this is in nature realized by O vacancies or donor atoms should be irrelevant for our model of the HH wall.

After setting up the supercell we optimized the atomic positions, subsequently the electronic structure of the supercell was analyzed. The layer-resolved density of states (DOS) of one domain is depicted in Fig. 2. The occupied Ti d state extends over nine layers close to the head-to-head domain wall. This means that the conductive layer is not localized at the domain wall but extends almost 7 nm.

Experimentally, no electronic conductivity at the head-to-head domain wall was reported. One way for recovering a globally insulating behavior is localizing the electrons at the transition metal atom ($Ti^{+4} \rightarrow Ti^{+3}$). As will be shown in the following, this localization is driven by strong Coulomb interaction and is assisted by $KCuF_3$-type distortions around the transition metal atoms. This mechanism leads to a complete

split-off of one of the Ti t_{2g} states from the bottom of the conduction band, so that a band gap opens. Since $KCuF_3$-type distortions cannot be accommodated in a p(1×1) geometry, we will consider c(2×2) unit cells in the following.

B. c(2×2) unit cells

We constructed a thin film of 13-layer thickness with PbO termination and $z \rightarrow -z$ mirror symmetry. The mirror plane is placed at the head-to-head domain (see Fig. 1). The atomic positions in thin film were initialized with the relaxed positions of the bulk tetragonal structure with a polarization which is pointing in the $\pm z$ direction towards the mirror plane. For compensating the polarization charges at the film surfaces, one electronic charge defect was created by replacing a single O by F in each surface unit cell. A similar situation is obtained by the creation of a single O vacancy per p(2×2) unit cell [24].

On the other hand, to compensate the polarization charges at the head-to-head domain wall, two electrons on two Ti atoms were localized at the domain wall by adding an on-site Coulomb repulsion term (characterized by a Hubbard parameter U) on the d states of all Ti atoms in the film. Here, the simulation is guided by the studies of other Ti^{3+} systems, e.g., $LaTiO_3$, where an orbital polarization and accompanying gap opening is observed for a value of U between 5 and 6 eV [25]. Other DFT+U studies of single, localized Ti d electrons, e.g., at polar/nonpolar interfaces applied U values ranging from 4 eV [26] to 8 eV [27]. In the electronically and structurally related $PbVO_3$, values between 3 and 6 eV gave reasonable agreement with more advanced functionals and experiment [28]. Since we have, apart from the observation that our studied domain walls are nonconducting, no experimental data to compare with, we can only scan a range of U values and observe, where the Ti d state splits off the conduction band. However, one should keep in mind that this value might be overestimated due to the underestimation of the band gap in the DFT calculation.

We varied U_d^{Ti} between 4.0 and 6.0 eV and fixed Hund's exchange parameter J to 0.7 eV. For each U_d^{Ti}, the thin-film structure was optimized and the DOS, ferroelectric distortion (δ_{FE}), and Ti $2p$ core-level energy of the thin films were calculated. Here, δ_{FE} for TiO_2^{II} and PbO^{I} layers is defined as $\delta_z(\mathrm{Ti}) - \delta_z(\mathrm{O^{II}})$ and $\delta_z(\mathrm{Pb}) - \delta_z(\mathrm{O^{I}})$, respectively. As the split-off state can be spin polarized, different magnetic configurations have to be investigated in the calculations.

The density of states in Fig. 3 show that the (ferromagnetic) structures for $U_d^{\mathrm{Ti}} < 4$ eV, 4 eV$> U_d^{\mathrm{Ti}} < 5$ eV, and $U_d^{\mathrm{Ti}} > 5$ eV were metallic, half metallic, and insulating, respectively. We observe magnetic ordering with a small magnetic moment of $0.5\mu_{\mathrm{B}}$ for the DFT calculation ($U = 0$), while for $U = 4$ eV the moment is already almost $1\mu_{\mathrm{B}}$. When a finite bandgap has developed, the magnetic moment is of course exactly unity.

Figure 4(a) depicts the ferroelectric distortion (δ_{FE}) for each layer in one of the domains of the thin films for different U_d^{Ti}. We observe the transition from a structurally smooth to a sharp domain wall with a critical U_d^{Ti} between 4 and 5 eV. Recent high-resolution transmission electron microscopy (HR-TEM) measurements indeed reported a longitudinal domain wall that shows a gradual change of the polarization over several nanometers. This can be reconciled with the model of strongly localized d electrons if we allow for a spatial distribution of the Ti^{3+} over several layers, in contrast to the (electrostatically unfavorable) accumulation in a single layer as assumed in our model.

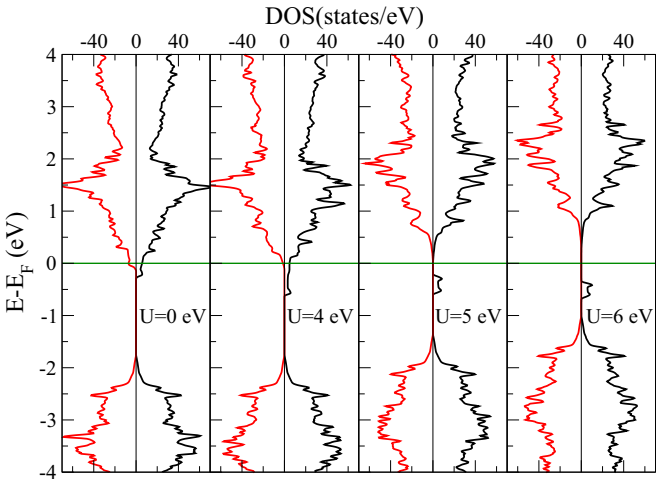

FIG. 3. (Color online) Density of states (DOS) of the two domains and the head-to-head domain wall in $PbTiO_3$ with different Hubbard U on the Ti d states. Gray (red) and black lines (negative and positive DOS values) represent minority and majority DOS, respectively.

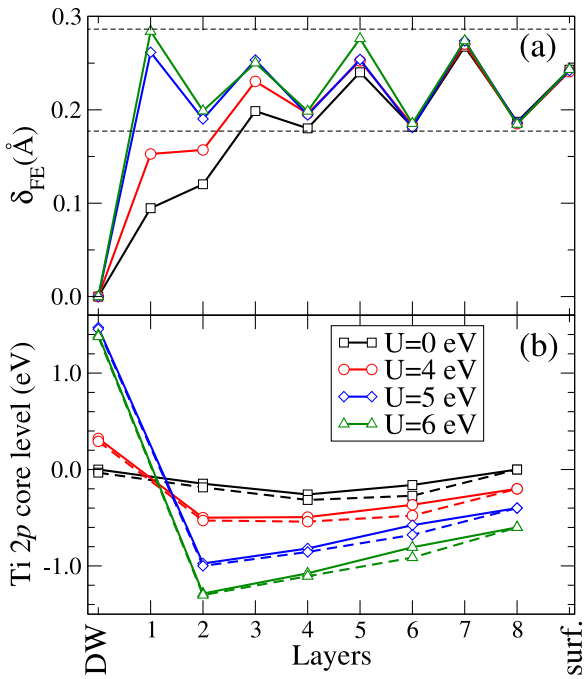

FIG. 4. (Color online) (a) Calculated ferroelectric distortion (δ_{FE}) in different layers of the head-to-head domain wall (DW) in $PbTiO_3$ for varying Hubbard U on Ti d states. Since the introduced surface charge is 62% smaller than what would be expected from the bulk polarization, the ferroelectric distortions are accordingly smaller. The dashed lines indicate the bulk values (scaled by 0.62) of the ferroelectric distortions for the PbO and TiO_2 planes. (b) Ti $2p$ core-level energies for different U. The core-level energies at the surface are fixed for $U = 0$ eV to 0; lines have been shifted by 200 meV for visibility.

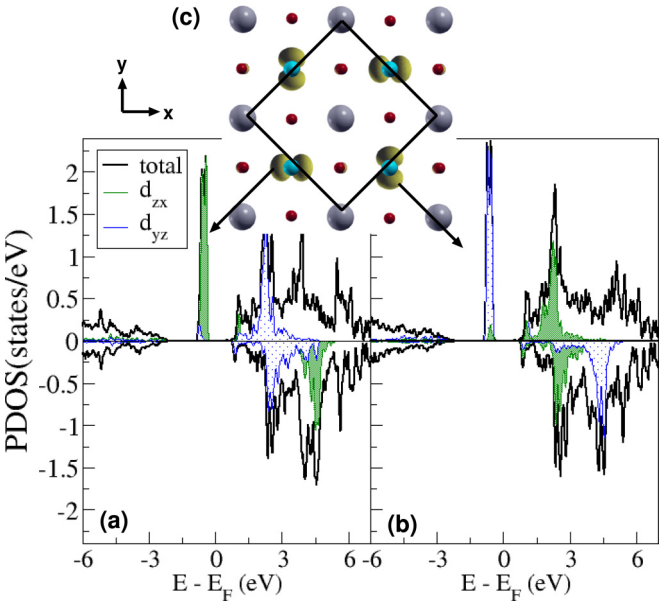

FIG. 5. (Color online) (a) and (b) Orbital-resolved density of states of the Ti atoms in a head-to-head domain wall in $PbTiO_3$ in c(2×2) geometry. Curves outlining the filled or shaded areas correspond to d_{zx} or d_{yz} orbital contributions, respectively. Notice that the ferroelectric polarization is directed along the z axis, therefore we see the electrons localize on d_{zx} (Ti_1) and d_{yz} (Ti_2) when a Hubbard U of 5.5eV is applied on the Ti d states. (c) Electron density (yellow) localized in the TiO_2 layer at head-to-head domain wall. Large (gray), small (red), and medium-sized (blue) spheres represent Pb, O, and Ti atoms, respectively.

The transition from a smooth to a sharp domain wall with increasing U_d^{Ti} is also visible electronically in the Ti $2p$ core-level shifts that are presented in Fig. 4(b), where only the majority spin channels of the $2p$ core-level energies are shown. The difference of the $2p$ core-level energies of the two spin channels is (for Ti^{+3}) about 0.2 eV. For $U_d^{\mathrm{Ti}} = 0$ eV, the core-level shifts between the Ti atoms in the domain wall and the Ti atoms at other layers are small (about 0.15 eV). In contrast, these shifts increase for $U_d^{\mathrm{Ti}} = 5$–6 eV (shifts between Ti^{+3} and neighboring Ti^{+4}) to about +2.5 eV. This value can be compared to the experimentally determined core-level shift between TiO_2 and Ti_2O_3 that amounts to roughly +1 eV [29].

In Fig. 5 the orbital-resolved d-DOS of the Ti atoms at the head-to-head domain wall with $U_d^{\mathrm{Ti}} = 5.5$ eV is shown. This DOS and the corresponding charge density near the Fermi energy [see Fig. 5(c)] shows an orbital ordering at the central (domain wall) layer. Each atomic Ti site is occupied by one electron in the d levels. Here, the d_{yz} and d_{zx} orbitals accommodate the two electrons at the Ti_1 and Ti_2 sites; therefore, the TiO_6 octahedron is distorted. When an electron is accommodated at a d_{yz} orbital, the TiO_6 octahedron is elongated in the y direction and contracted in the x direction. This distortion is the opposite way when an electron is localized on a d_{zx} orbital. This distortion (expressed as the difference of the Ti-O bond length in the two directions) amounts to 0.09 Å for $U_d^{\mathrm{Ti}} = 5.5$ eV.

In addition, different magnetic orderings, i.e., ferromagnetic (FM) and antiferromagnetic (AFM), were considered at the domain wall. We find that the FM state is energetically more favorable than the AFM ordering: For U_d^{Ti} ranging from 4.5 to 6 eV, the energy difference E_{AFM}-E_{FM} changes from 75 to 29 meV. We see that larger values of U lead to stronger localization and reduced hopping, resulting in a smaller exchange interaction.

Up to now, we considered (bulk) polarizations that are compatible with the existence of one additional electron/hole per unit cell at the domain walls. As the ferroelectric polarization varies for different materials or as it can be changed in thin films by the defect concentration at the surface, it is important to know how the electronic structure at the domain wall is manipulated by varying the ferroelectric polarization. For example, there is experimental data showing a change of ferroelectric polarization P with varying oxygen partial pressure at the surface [17]. A question arising in this context is now whether the electrons at the domain wall always remain localized, or, below a critical P, form an extended state or electron gas.

In the following, we keep U_d^{Ti} fixed at 5.5 eV for all Ti atoms and simulate different ferroelectric polarizations by varying the defect concentration at the tails of the domains. In our film model, where the HH domain wall is located at the center of the film, this means that we vary the concentration of charged defects at the surface between $0.3e^-$ and $1.0e^-$ per c(2×2) in-plane unit cell. Consequently, the charge accumulating in the domain wall is $0.3-1.0e^-$ per Ti atom. The charge defects on the surface were simulated by the virtual crystal approximation [i.e., the nuclear and electron number of the atoms at the O sites was varied smoothly between 8 (O) and 9 (F)] and the thin-film structure was optimized. Figure 6(a) shows the relation between surface defect concentration and ferroelectric distortion in the layers of the thin film. We further calculated the local Ti DOS at the domain wall for each optimized structure (cf. Fig. 7) finding that the electronic structure at the domain wall can be modified from insulating to conducting by a small change of P, i.e., by changing the defect concentration on the surface. This result is in agreement with theoretical investigations of Sr-doped $LaTiO_3$ [25]. Qualitatively, we see that beyond a critical concentration the electrons at the DW tend to localize on a Ti d band. In cases of integer filling (1.0 and 0.5 e^-/surface unit cell), we observe an insulating ground state, while in between metallic phases are observed (Fig. 7). However, we can expect that the insulating regime extends much further and the observed metallicity is just a size effect from the c(2×2) unit cell. We will discuss this aspect in the next section for the p(2×2) geometry.

In Fig. 6 we show the ferroelectric distortion (δ_{FE}) for each layer of the thin films for different defect concentrations. We find that not only δ_{FE} decreases by reducing the defect concentration, there is also a transition to an extended domain wall for $0.3e^-$ charge defects indicating delocalization of the Ti $2d$ electrons. This is also visible in the Ti $2p$ core-level shifts presented in Fig. 6(b) for different charge defects on surfaces. The core-level shifts between Ti atoms at the domain wall increase by decreasing charge defects at the surface. Below $0.3e^-$ per surface unit cell the screening charge is delocalized and the core level shifts (CLSs) for both central Ti atoms are

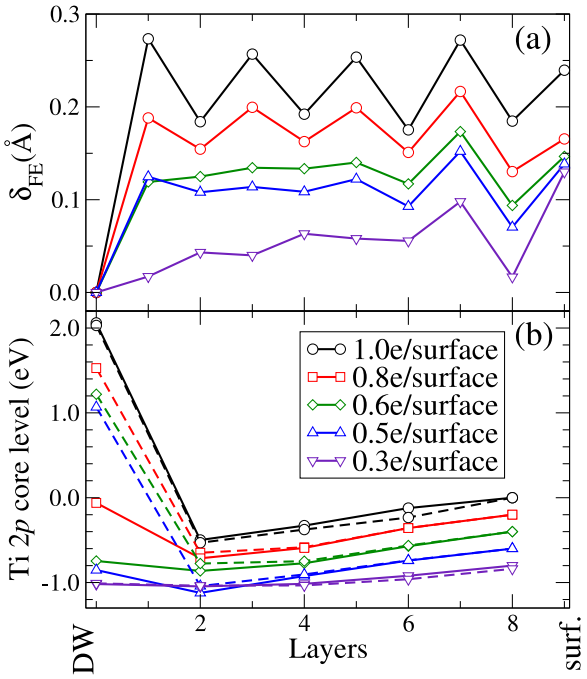

FIG. 6. (Color online) (a) Calculated ferroelectric distortion (δ_{FE}) at different layers of the head-to-head domain wall (DW) in $PbTiO_3$ with the fixed $U_d^{Ti} = 5.5$ eV and varying defect concentration at the thin-film surface. (b) Ti $2p$ core-level energies for these defect concentrations at the thin-film surface. The core-level energies at the surface are fixed for 1 electron/surface concentration to 0 meV; lines have been shifted by 200 meV for visibility. Solid and dashed lines represent the two different Ti atoms, Ti_1 and Ti_2 in Fig. 5(c), at each layer, respectively.

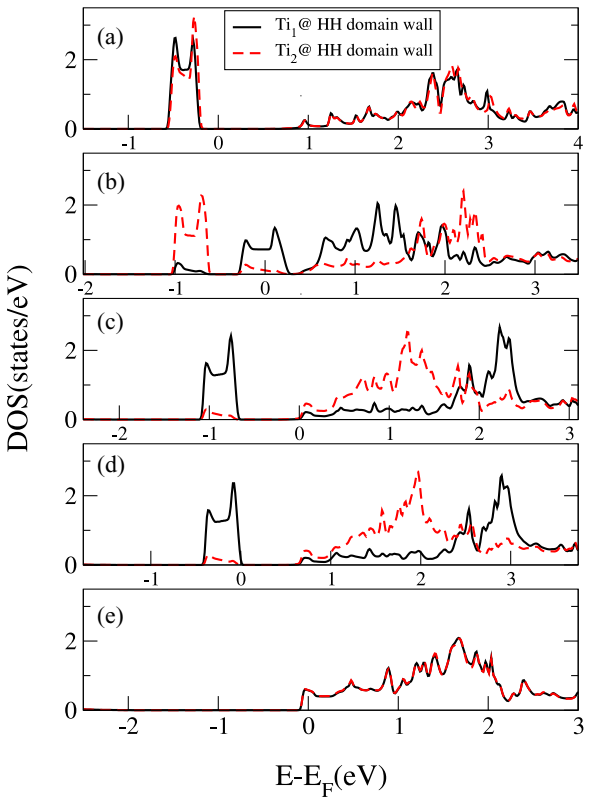

FIG. 7. (Color online) Majority density of states of Ti at the head-to-head domain wall in $PbTiO_3$ for different defect concentration at the thin-film surface: Panels (a)–(e) show the local DOS for 1, 0.8, 0.6, 0.5, and 0.3 electron defects per c(2×2) surface unit cell, respectively.

similar. Beyond $0.5e^-$ per unit cell one electron localizes on one of the Ti atoms and the CLS amounts to almost 2 eV for that atom. For one electron per unit cell, both Ti get equivalent again and show a large CLS.

C. p(2×2) unit cells

To identify artifacts in the above analysis that come from the size constraint of the c(2×2) unit cell, we studied the localization and orbital order on Ti at domain walls in p(2×2) geometry. For this purpose, we constructed a thin film of $PbTiO_3$ of seven-layer thickness. In this setup, we choose the same termination and mirror symmetry as in the c(2×2) geometry. The concentration of the charge defects at the p(2×2) thin-film surface was varied from $1.5e^-$ to $1e^-$ and $0.5e^-$ per in-plane unit cell. Again, the charge defects on the surface were simulated by the virtual crystal approximation. On the other hand, the polarization charges at the domain wall which are induced by the polarization are compensated by a change of the Ti valency (localization of an electron on Ti assisted in the DFT calculation by a Hubbard U). In this geometry there are four Ti atoms at the domain wall. For $1.5e^-$, $1e^-$, and $0.5e^-$ defects at the surface the valency of three, two, and one Ti at the domain wall was changed, respectively. U_d^{Ti} was again fixed to 5.5 eV and the structure of the thin film was optimized. For each defect concentration insulating behavior was observed. The gap in these configurations is smaller than that of the c(2×2) cell with the $0.5e^-$ or $1e^-$ defect. One should note, that the concentrations of the $1.5e^-$ and $0.5e^-$ defects would correspond to $0.25e^-$ and $0.75e^-$ per c(2×2) surface unit cell and hence we find that metallic behavior is suppressed and that also in these cases the correlation effect can introduce split-off states within the gap. Thus, charge-ordered states keep the structure insulating. Nevertheless, we also see that the gap shrinks in Fig. 7 from (a) to (d) for a fixed value of U and below a certain electron concentration, a transition to metallic behavior can be expected. However, the details of this metal-to-insulator transition might actually be very complex as the decreasing concentration of Ti^{+3} can counteract the decrease in the bandgap and hence the band picture of conductance might not be appropriate in the limit of small gaps.

Moreover for two electrons in the p(2×2) unit cell of the domain wall, we investigated two different electronic structures at the Ti^{+3} atoms: First, one electron was localized on a d_{yz} orbital of Ti_1 and other one on the d_{zx} orbital of Ti_4 (cf. Fig. 8). In comparison the two electrons were localized on the same orbital type, e.g., d_{yz}, on Ti_1 and Ti_4. We found that the second electronic structure is more favorable than the first one by 94 meV per p(2×2) unit cell. This type of orbital ordering is different from the one obtained by DFT+U calculations of the two-dimensional electron gas at the $LaAlO_3/SrTiO_3$ interface, where a d_{xy} orbital was occupied at every second Ti site [27].

At the head-to-head domain wall of $PbTi_3$, also for three Ti^{+3} atoms in the p(2×2) unit cell, strong orbital-ordering

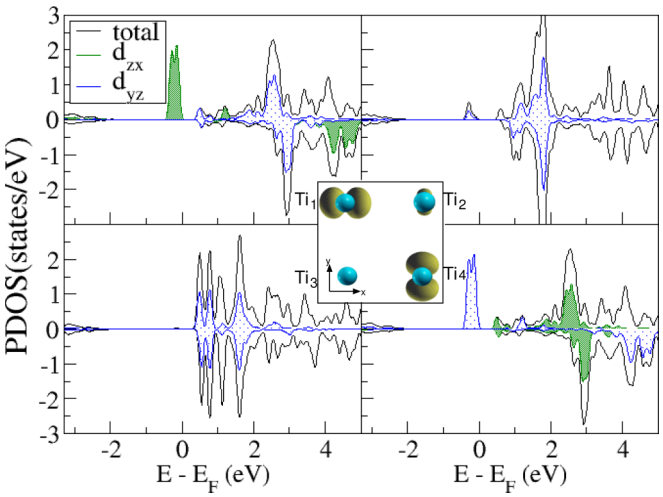

FIG. 8. (Color online) Orbital resolved density of states of Ti at a head-to-head domain wall in $PbTiO_3$, the p(2×2) geometry with a Hubbard U of 5.5 eV on the Ti d states. The orbital contribution of the d_{zx} and d_{yz} orbitals is indicated by filled and shaded curves, respectively. In the inset, (blue) spheres represent Ti atoms and the yellow lobes represent the electrons which are localized on Ti.

effects were observed, again with alternating d_{zx} and d_{yz} orbitals as nearest neighbors.

IV. CONCLUSIONS

The atomic and electronic structure of longitudinal domain walls in $PbTiO_3$ stabilized by charge compensating defects was investigated from first principles. The tail-to-tail domain walls (in supercell geometry) or the tails of the domains (in thin-film setup) were stabilized by F atoms replacing O or oxygen defects. At the resulting head-to-head domain wall, one electron is accommodated by the Ti d band. Simulating strong correlation effects by inclusion of a static Hubbard U, we find a metal-to-insulator transition at a critical U of about 5 eV. The calculation of magnetic configurations at the domain walls with one electron per Ti atom in the central layer showed that the ferromagnetic configuration is energetically more favorable than the antiferromagnetic one. Although this insulating domain-wall model is—in contrast to recent HR-TEM investigations—atomically sharp (the ferroelectric displacements revert across the interface within two unit cells), one can assume that in the realistic head-to-head domain wall with a more extended distribution of Ti^{+3} sites over several layers similar localization effects should occur resulting in insulating domain walls.

While these structures are very similar to those at interfaces between different polar insulators, the use of ferroelectric materials in principle enables one to tune the interface or domain wall by varying the ferroelectric polarization. The resulting changes of the electronic structure of the head-to-head domain wall were also investigated and complex charge- and orbital-ordering effects have been found. Although our model for on-site correlation is a simple frequency-independent method, it can be expected to capture this part of the complexity to some extent. In particular, our investigation suggests that the insulator-metal transition in Ti oxides is not necessarily sharp; charge- and orbital-ordering effects allow a variation of the electron concentration without losing the insulating properties of the system within a certain range.

ACKNOWLEDGMENTS

Research leading to these results has received funding from the European Community's Seventh Framework Programme (FP7/2007-2013) under Grant Agrement No. NMP3-LA-2010-246102 and the Deutsche Forschungsgemeinschaft (SFB 917). We gratefully acknowledge computing time at the JUROPA supercomputer from the Jülich Supercomputing Centre.

[1] A. Ohtomo and H. Y. Hwang, Nature (London) **427**, 423 (2004).
[2] J. Seidel, L. W. Martin, Q. He, Q. Zhan, Y.-H. Chu, A. Rother, P. Hawkridge, P. Maksymovych, M. Yu, N. Gajek, S. V. Balke, S. Kalinin, F. Gemming, M. E. Wang, G.and Catalan, J. F. Scott, N. A. Spaldin, J. Orenstein, and J. Ramesh, Nature Mater. **8**, 229 (2009).
[3] S. Ohta, T. Nomura, H. Ohta, M. Hirano, H. Hosono, and K. Koumoto, Appl. Phys. Lett. **87**, 092108 (2005).
[4] B. Jalan and S. Stemmer, Appl. Phys. Lett. **97**, 042106 (2010).
[5] Y. Inoue, K. Sato, K. Sato, and H. Miyama, J. Phys. Chem. **90**, 2809 (1986).
[6] A. Kudo, Catal. Survey Asia **7**, 31 (2003).
[7] J. L. Giocondi and G. S. Rohrer, J. Phys. Chem. B **105**, 8275 (2001).
[8] N. V. Burbure, P. A. Salvador, and G. S. Rohrer, Chem. Mater. **22**, 5823 (2010).
[9] Y. Zhang, A. M. Schultz, P. A. Salvador, and G. S. Rohrer, J. Mater. Chem. **21**, 4168 (2011).
[10] L. Li, Y. Zhang, A. M. Schultz, X. Liu, P. A. Salvador, and G. S. Rohrer, Catal. Sci. Technol. **2**, 1945 (2012).
[11] I. Krug, N. Barrett, A. Petraru, A. Locatelli, T. O. Mentes, M. A. Nino, K. Rahmanizadeh, G. Bihlmayer, and C. M. Schneider, Appl. Phys. Lett. **97**, 222903 (2010).
[12] T. M. Shaw, S. Trolier-McKinstry, and P. C. McIntyre, Ann. Rev. Materials Sci. **30**, 263 (2000).
[13] J. Paul, T. Nishimatsu, Y. Kawazoe, and U. V. Waghmare, Phys. Rev. Lett. **99**, 077601 (2007).
[14] J. Junquera and P. Ghosez, Nature (London) **422**, 506 (2003).
[15] J. E. Spanier, A. M. Kolpak, J. J. Urban, I. Grinberg, L. Ouyang, W. S. Yun, A. M. Rappe, and H. Park, Nano Letters **6**, 735 (2006).
[16] D. D. Fong, A. M. Kolpak, J. A. Eastman, S. K. Streiffer, P. H. Fuoss, G. B. Stephenson, C. Thompson, D. M. Kim, K. J. Choi, C. B. Eom, I. Grinberg, and A. M. Rappe, Phys. Rev. Lett. **96**, 127601 (2006).

[17] R. V. Wang, D. D. Fong, F. Jiang, M. J. Highland, P. H. Fuoss, C. Thompson, A. M. Kolpak, J. A. Eastman, S. K. Streiffer, A. M. Rappe, and G. B. Stephenson, Phys. Rev. Lett. **102**, 047601 (2009).
[18] D. D. Fong, G. B. Stephenson, S. K. Streiffer, J. A. Eastman, O. Auciello, P. H. Fuoss, and C. Thompson, Science **304**, 1650 (2004).
[19] C.-L. Jia, S.-B. Mi, K. Urban, I. Vrejoiu, M. Alexe, and D. Hesse, Nature Mater. **7**, 57 (2008).
[20] G. Catalan, J. Seidel, R. Ramesh, and J. F. Scott, Rev. Mod. Phys. **84**, 119 (2012).
[21] X. Wu and D. Vanderbilt, Phys. Rev. B **73**, 020103 (2006).
[22] Z. Wu and R. E. Cohen, Phys. Rev. B **73**, 235116 (2006).
[23] FLEUR http://www.flapw.de/.
[24] K. Rahmanizadeh, G. Bihlmayer, and S. Blügel (unpublished).
[25] A. Liebsch, Phys. Rev. B **77**, 115115 (2008).
[26] R. Oja, M. Tyunina, L. Yao, T. Pinomaa, T. Kocourek, A. Dejneka, O. Stupakov, M. Jelinek, V. Trepakov, S. van Dijken, and R. M. Nieminen, Phys. Rev. Lett. **109**, 127207 (2012).
[27] R. Pentcheva and W. E. Pickett, Phys. Rev. B **74**, 035112 (2006).
[28] A. S. Milošević, M. V. Lalić, Z. S. Popović, and F. R. Vukajlović, Optical Materials **35**, 1765 (2013).
[29] L. T. Hudson, R. L. Kurtz, S. W. Robey, D. Temple, and R. L. Stockbauer, Phys. Rev. B **47**, 1174 (1993).